J. Fluid Mech. (2014), *vol.* 741, *pp* 200–227.
doi:10.1017/jfm.2013.562

Breakdown of the Bretherton law due to wall slippage

Yen-Ching Li[1], Ying-Chih Liao[2], Ten-Chin Wen[1] and Hsien-Hung Wei[1,†]

[1]Department of Chemical Engineering, National Cheng Kung University, Tainan 701, Taiwan

[2]Department of Chemical Engineering, National Taiwan University, Taipei 10617, Taiwan

(Received 31 January 2013; revised 30 September 2013; accepted 20 October 2013; first published online 7 February 2014)

Against the common wisdom that wall slip plays only a minor role in global flow characteristics, here we demonstrate theoretically for the displacement of a long bubble in a slippery channel that the well-known Bretherton 2/3 law can break down due to a fraction of wall slip with the slip length λ much smaller than the channel depth R. This breakdown occurs when the film thickness h_∞ is smaller than λ, corresponding to the capillary number Ca below the critical value $Ca^* \sim (\lambda/R)^{3/2}$. In this strong slip regime, a new quadratic law $h_\infty/R \sim Ca^2(R/\lambda)^2$ is derived for a film much thinner than that predicted by the Bretherton law. Moreover, both the 2/3 and the quadratic laws can be unified into the effective 2/3 law, with the viscosity μ replaced by an apparent viscosity $\mu_{app} = \mu h_\infty/(\lambda + h_\infty)$. A similar extension can also be made for coating over textured surfaces where apparent slip lengths are large. Further insights can be gained by making a connection with drop spreading. We find that the new quadratic law can lead to $\theta_d \propto Ca^{1/2}$ for the apparent dynamic contact angle of a spreading droplet, subsequently making the spreading radius grow with time as $r \propto t^{1/8}$. In addition, the precursor film is found to possess $\ell_f \propto Ca^{-1/2}$ in length and therefore spreads as $\ell_f \propto t^{1/3}$ in an anomalous diffusion manner. All these features are accompanied by no-slip-to-slip transitions sensitive to the amount of slip, markedly different from those on no-slip surfaces. Our findings not only provide plausible accounts for some apparent departures from no-slip predictions seen in experiments, but also offer feasible alternatives for assessing wall slip effects experimentally.

Key words: coating, interfacial flows (free surface), lubrication theory, thin films

1. Introduction

In the standard texts of fluid mechanics, it is commonly assumed that a fluid has no relative motion with respect to a solid boundary. This no-slip condition has its rationale in that the inevitable friction on a surface can bring the nearby fluid to rest. It is also the condition that ensures steady flow, since viscous drag can be generated by sharp velocity gradients on solid boundaries to counterbalance the applied forcing. While the no-slip condition has been widely used in many practical flows, considerable wall slip, intrinsic or apparent, might exist in a number

†Email address for correspondence: hhwei@mail.ncku.edu.tw

of occasions. Typical examples are polymer solutions flowing over surfaces (de Gennes 1979), pumping in hydrophobic microchannels with/without surface structures (Tretheway & Meinhart 2002; Choi *et al.* 2006; Tsai *et al.* 2009), draining on chemically decorated substrates (Craig, Neto & Williams 2001; Zhu & Granick 2001), and coating on uneven/structured plates (Krechetnikov & Homsy 2005; Seiwert, Clanet & Quéré 2011).

Slip effects are often characterized by the Navier slip condition (Navier 1823):

$$u = \lambda \frac{\partial u}{\partial y}, \tag{1.1}$$

where the slip length λ can be defined as the ratio of the slip velocity to the local shear rate. As the actual no-slip point can be located by extrapolating to the zero-velocity plane outside the slip surface, λ can therefore be interpreted as the distance from that point to the surface. With the above picture in mind, (1.1) immediately reveals that $\lambda = 0$ recovers the usual no-slip condition and that $\lambda = \infty$ allows complete slip in a stress-free manner, $\partial u/\partial y = 0$. Depending on the molecular/microscopic nature of a surface, λ can range from 10 nm to 10 μm (Lauga, Brenner & Stone 2007). Thus, wall slip, if it exists, would become much more apparent at submicron or nanometre scales. Perhaps the most frequent use of the Navier condition (1.1) occurs in modelling dynamic wetting in order to relieve the stress singularity at the moving contact line (Hocking 1976; Cox 1986). In most situations, λ is much smaller than the liquid thickness h. So slip effects are only important near the contact line and do not change the macroscopic flow characteristics (see Bonn *et al.* 2009 for a more comprehensive review). While the above is generally true for smooth surfaces whose intrinsic slip lengths are of about molecular sizes or nanometre scales (Bocquet & Barrat 2007), there exist situations where apparent slip lengths are large, for instance, flows of polymeric liquids (de Gennes 1979), spreading on less viscous pre-wetting films (Brochard-Wyart, Debrégeas & de Gennes 1996), and imbibition on porous surfaces (Beavers & Joseph 1967). In this case, λ can be so large that slip effects do not merely affect the local flow field but the global one, causing the entire flow to speed up by a factor of λ/h. What is more important is that this flow amplification might significantly modify how the fluid–fluid interface behaves both spatially and temporally in response to such a very slippery flow. So for the systems mentioned above, we anticipate that the flow characteristics would differ quantitatively from those on no-slip surfaces.

Motivated by the above, in this paper we pay particular attention to how wall slip affects thin film coating processes. One important class of coating flows is deposition of a thin film on the interior wall of a small capillary by displacing liquid with a long bubble. This is the classical Bretherton problem (Bretherton 1961). A similar film deposition can also be realized by withdrawing a plate from a bath of liquid, the so-called Landau–Levich dip coating (Landau & Levich 1942), which was known long before Bretherton's work. For coating flows of this sort, it is well known that the deposited film thickness scales like the 2/3 power of the coating speed – the classical Bretherton law (Bretherton 1961). This result is based on the no-slip boundary condition commonly assumed for solid surfaces. Just like flow near the contact line in dynamic wetting problems, we anticipate that introduction of the additional slip length might also change the flow characteristics for the Bretherton problem. But it is not clear whether the film is thickened or thinned by such a change, nor how the Bretherton 2/3 law is modified due to wall slippage. These two questions will be addressed in this paper. In addition, we will look into how the

coating behaviour is characterized by the amount of wall slip under the strong slip situation, relevant to situations involving polymeric liquids, heterogeneous surfaces, and coating over pre-wetting films mentioned above.

In terms of experiments, there does exist some evidence showing violation of the Bretherton law. Seiwert *et al.* (2011) performed dip coating over a plate textured with micropillars and found that the deposited film thickness is systematically thicker than the Bretherton law. Specifically, the film thickness approaches the Bretherton law at high plate withdrawal velocities whereas it approaches a constant in the low velocity regime. This observation can be interpreted by the fact that part of the wetting liquid is trapped within the interspace of the pillars, giving rise to an increase in the viscous drag on the liquid and therefore thickening the film. But when the liquid thickness becomes comparable to the pillar height, this film thickening becomes saturated, causing the film thickness to no longer vary with the plate velocity. In a related work, Krechetnikov & Homsy (2005) examined surface roughness effects on dip coating processes. They found that the film thickness appears to be slightly thicker and shows a slower power-law dependence on the plate pulling speed compared to the Bretherton law. They also introduced an apparent slip length in their model to explain the role played by slip effects. These studies seem to imply that the Bretherton law still holds when the sizes of the surface structures are small compared to the film thicknesses. In fact, the observed film thickening phenomena can actually be interpreted in terms of negative slip length in the sense that the surface structures impart more viscous dissipation to slow down the fluid motion.

Another motivation for this work comes from the need to measure slip length experimentally. Common techniques involve measurement of pressure drop (Choi, Westin & Breuer 2003), particle image velocimetry (Tretheway & Meinhart 2002), squeeze flow rheometry (Zhu & Granick 2001), surface force apparatus (Restagno *et al.* 2002), and so on. Among these, the last two appear to be more reliable approaches because one can use a solid probe to extract the slip length of a surface by analysing how the force on the probe responds in the near-contact situation. However, such a force does not change appreciably with the amount of slip, especially when the probe–surface distance is smaller than the slip length (Vinogradova 1995). Inspired by the Bretherton problem that the film thickness can be controlled by the coating speed, perhaps a better way to render a greater hydrodynamic susceptibility to probing slip boundaries is to inject a long bubble into a confined channel or to simply withdraw a plate from a bath of liquid. By identifying how the measured film thickness deviates from the Bretherton law, one might be able to determine the slip length more accurately.

In addition to coating and measuring slip length, the Bretherton problem with slip walls is also relevant to gas–liquid slug flows seen in microfluidic devices (Song, Tice & Ismagilov 2003; Oskooei & Sinton 2010). On the one hand, wall slip can reduce drag to facilitate transport of these slugs. On the other hand, trailing films on the gas side could become so thin that they might be more inclined to be in contact with the channel walls to impede the motion of slugs. Therefore, it is necessary to understand the role played by wall slip in such a system so that one can optimize the transport without clogging the channels.

We have recently demonstrated that wall slippage can drastically modify hydrodynamics for a wide class of interfacial flows (Liao, Li & Wei 2013). In this paper we will give a more detailed account of how wall slip impacts the Bretherton problem. Using both scaling theory and lubrication analysis in §§ 2 and 3, we will show how the Bretherton 2/3 law breaks down when wall slip effects become

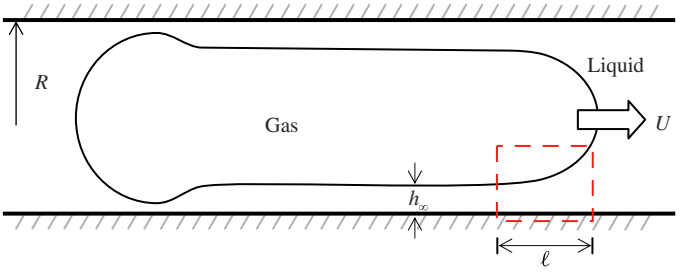

FIGURE 1. (Colour online) Flow geometry for the motion of a long, closely fitting bubble in a channel. Here we focus on the transition region between the front meniscus and the uniform film region, as indicated by the box.

important at sufficiently low bubble speeds. In addition, a new quadratic law will be derived to characterize the behaviour of the film thickness in this strong slip regime, accompanied by the unique no-slip-to-slip transition between these two laws. In § 4 we extend the analysis to textured surfaces. This part will not only provide a link between apparent slip length and apparent viscosity, but also show how we unify both the 2/3 and the quadratic laws. We also show in § 5 that more insights and perspectives can be found by making connections to dip coating and drop spreading. In § 6, at the micro/mesoscale level, we make further connections between slip length and molecular length arising from disjoining pressure, and demonstrate how both determine a new precursor film structure in drop spreading. These connections can possibly explain a number of apparent deviations from no-slip predictions seen in experiments. The paper is concluded in § 7.

2. The Bretherton problem with slip walls: scaling theory

Figure 1 shows the flow geometry of the problem. A closely fitting, long air bubble is moving at constant velocity U in a two-dimensional channel of depth $2b$. The liquid is an incompressible Newtonian fluid of viscosity μ. The air–liquid interface is assumed to be clean and has uniform surface tension σ. The bubble displacement leads to a deposition of thin films of yet to be determined thickness $h_\infty (\ll b)$ on the channel walls. There also exists a non-uniform transition zone of length $\ell \sim (h_\infty R)^{1/2}$ between the uniform film and the round bubble front having radius of curvature $R (\approx b)$. The goal here is to investigate how h_∞ varies with both the bubble speed U and the slip length λ.

2.1. *Dimensional analysis*

We start with a dimensional/scaling analysis to gain some insights prior to solving the problem in detail. We restrict our attention to viscosity-dominated flow with negligible inertial effects, so that the problem here is independent of the fluid density. As a result, the problem can be characterized by six independent variables: h_∞, R, λ, U, μ and σ. A simple dimensional analysis reduces them to three dimensionless parameters and suggests the following form for h_∞ in terms of the remaining variables:

$$\frac{h_\infty}{R} = f\left(\frac{\mu U}{\sigma}, \frac{\lambda}{R}\right), \tag{2.1}$$

where $\mu U/\sigma$, the ratio of viscous to surface tension effects, is often called the capillary number Ca and typically very small compared to unity. Note that we do not include $\ell \sim (h_\infty R)^{1/2}$ in (2.1) in view of its purely geometric connection to h_∞ and R.

As we expect that h_∞ should grow with U (because of much stronger flow injection into the film) but become thinner due to λ (because of much stronger capillary draining out of the film), we postulate that (2.1) follows the power law

$$\frac{h_\infty}{R} = c_1 Ca^n \left(\frac{R}{\lambda}\right)^m, \tag{2.2}$$

with c_1 being a numerical factor. The values of n (>0) and m ($\geqslant 0$) depend on the size of h_∞ relative to λ, which can be controlled by U (via Ca). In the no-slip ($h_\infty \gg \lambda$) limit, we should recover the well-known Bretherton law with $n = 2/3$ and $m = 0$.

In the strong slip limit ($h_\infty \ll \lambda$) at a very low U, although both n and m are not yet known, we can at least obtain some information about their values based on the following physical judgements. First of all, because the slip condition imparts additional fluid drainage (Vinogradova 1995), we expect the film thickness with slip to be thinner than that without slip. Moreover, because $Ca \ll 1$ and $R/\lambda > 1$, the film for the slip case should undergo more rapid thinning than the no-slip case as Ca decreases. This ensures that for $Ca \ll 1$ the film thickness in the former is always thinner than that in the latter, which requires $n > 2/3$. Alternatively, as λ gets smaller, a transition from no-slip to slip should occur at smaller Ca because we expect a much thinner film to see slip effects. The capillary number at the transition point Ca^* can be estimated by setting the Bretherton scale $h_\infty/R \sim Ca^{2/3}$ equal to (2.2),

$$Ca^* \sim \left(\frac{\lambda}{R}\right)^{m/(n-2/3)}, \tag{2.3a}$$

which necessitates $n > 2/3$ to ensure the smallness of Ca^*. In fact, Ca^* can be found by simply setting $h_\infty \sim R\, Ca^{2/3}$ to be λ without having to resort to actual scaling in the strong slip regime, giving $Ca^* \sim (\lambda/R)^{3/2}$ (see (2.11)) and hence

$$m = \tfrac{3}{2}n - 1. \tag{2.3b}$$

Below we will carry out a scaling analysis to determine n and m by deriving the scaling law for h_∞ in the strong slip regime.

2.2. *Flow mechanisms and new scaling laws*

Next, we explain flow mechanisms and carry out a scaling analysis to estimate physical quantities involved. To better understand how the film thickness is determined, it is instructive to first review the classical Bretherton problem in the no-slip limit. This will provide some physical perspective for the derivation of scalings in the strong slip limit.

2.2.1. *No-slip limit* ($h_\infty \gg \lambda$)

This limit can be considered when the film is much thicker than the slip length. Most of the discussion here closely follows the book by de Gennes, Brochard-Wyart & Quéré (2003) or the recent review by Stone (2010). Figure 2 depicts the basic flow mechanism. Here we focus on the transition region where the film thickness h

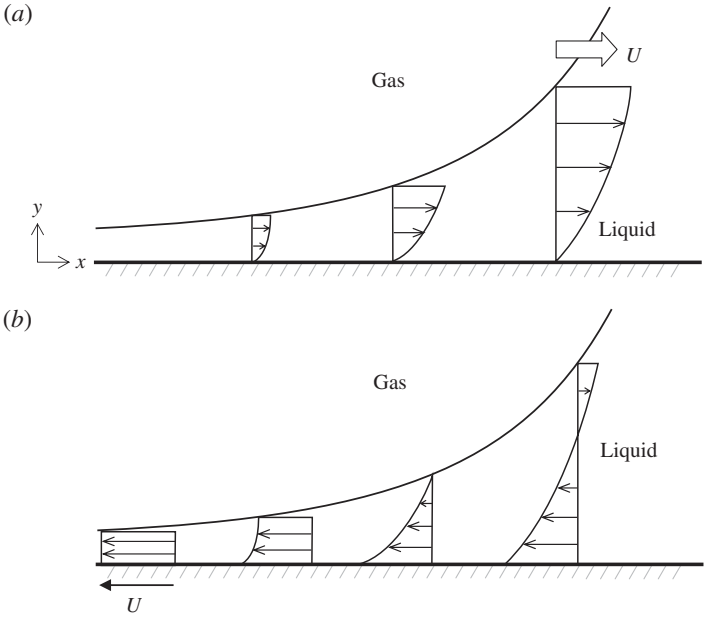

FIGURE 2. Flow mechanism for the Bretherton problem with no-slip walls. (*a*) The fixed frame, showing that capillary draining can develop out of the film during bubble displacement. (*b*) The frame moving with the bubble, showing fluid entrainment into the film because of the net flow injected by the bubble's sweeping.

has magnitude h_∞ and varies slowly with position. The very first idea begins with the following picture. While the fluid is drawn into the film due to the bubble's displacement, because the thicker part of the film has a greater interfacial curvature than the thinner part, this creates a negative capillary pressure $p \sim \sigma h_\infty/\ell^2$ to drain the fluid out of the film. Note here that the transition region has size $\ell \sim (h_\infty R)^{1/2}$ because the interface's curvature in this region h_∞/ℓ^2 has to match that of the bubble meniscus $1/R$.

The velocity u_{cap} of such capillary draining can be estimated by balancing the capillary pressure to the viscous stress along the flow direction, $p/\ell \sim \mu u_{cap}/h_\infty^2$, yielding

$$u_{cap} \sim \left(\frac{\sigma}{\mu}\right)\left(\frac{h_\infty}{\ell}\right)^3. \tag{2.4}$$

This capillary velocity must be of the same order of magnitude as the bubble velocity U. So we arrive at

$$\left(\frac{h_\infty}{\ell}\right)^3 \sim Ca. \tag{2.5}$$

If the fluid is allowed to flow in and out of the film continuously, the above condition will guarantee a uniform film deposition over the channel walls due to a slight mismatch between the capillary flow rate (per unit width) $q \sim u_{cap}h$ and the uniform sweeping Uh by the bubble displacement. It is also worth mentioning that in the context of forced wetting, (2.5) is essentially the Hoffman–Tanner law for perfectly

wetting liquids, $\theta_d^3 \sim Ca$ (Hoffman 1975; Tanner 1979), where $\theta_d \approx h_\infty/\ell$ is the apparent dynamic contact angle (de Gennes 1985; Stone 2010). Using $\ell \sim (h_\infty R)^{1/2}$, (2.5) then reduces to the well-known Bretherton law:

$$\frac{h_\infty}{R} \sim Ca^{2/3}. \tag{2.6}$$

Therefore it follows that the length of the transition region is $\ell \sim R\,Ca^{1/3}$.

It is tempting to determine the dynamic pressure difference Δp across the bubble so that one can know how much force is required to push the bubble at a given speed. This can be achieved by a macroscopic force balance. But it is not done over the entire bubble. Rather, it should be made over the transition region, which makes most of the contribution here. This is because the fluid around the two menisci are deemed to be virtually hydrostatic for small Ca and there is no viscous drag at all in the long uniform film region (Bretherton 1961). So the force balance over the transition region $\Delta pRW \sim (\mu U/h_\infty)\ell W$ (with W being the channel width) together with (2.6) gives

$$\Delta p \sim \frac{\sigma}{R} Ca^{2/3}. \tag{2.7}$$

This can actually be viewed as an $O(Ca^{2/3})$ correction to the capillary pressure around the bubble cap due to the film, namely, $\Delta p \sim (\sigma/R)(h_\infty/R)$. Independence of Δp of the bubble length in (2.7) is a direct consequence of the dominant contribution of the transition region to the macroscopic force balance.

2.2.2. *Strong slip limit* ($h_\infty \ll \lambda$)

The Bretherton law (2.6) indicates that h_∞ can be decreased by lowering Ca. So when Ca is decreased to the value (see (2.11)) where h_∞ is comparable or below the slip length λ, the Bretherton law breaks down and we enter the strong slip regime. Similar to the no-slip case discussed above, what happens in this regime can be pictured below. As depicted in figure 3, wall slip can promote capillary draining, making the film thinner. This is why the slip condition is often used to describe the water repelling effect on hydrophobic surfaces (Vinogradova 1995). When this effect is strong and the bubble speed is sufficiently low, the film can become so thin that it starts to see slip effects within λ. In this case, the capillary velocity can be amplified by a factor of λ/h_∞ according to (1.1):

$$u'_{cap} \sim \lambda \frac{u_{cap}}{h_\infty}. \tag{2.8}$$

It is worth remarking that such slip-induced flow amplification is realized for stress-free interfaces as considered here. The situation here is somewhat similar to pressure-driven flow in a slippery capillary tube in which the maximum velocity along the centreline can be increased due to wall slippage (Lauga & Stone 2003). A similar idea can also work to increase the effective slip velocities in diffusio-osmosis and electro-osmosis (Ajdari & Bocquet 2006).

Following (2.8), we again take $u'_{cap} \sim U$ to estimate h_∞, yielding

$$\left(\frac{h_\infty}{\ell}\right)^3 \sim Ca\left(\frac{h_\infty}{\lambda}\right) \quad \text{or} \quad \left(\frac{h_\infty}{\ell}\right)^2 \sim Ca\left(\frac{\ell}{\lambda}\right). \tag{2.9}$$

Compared to (2.5) in the no-slip limit, the dynamic contact angle relationship is modified by lowering Ca by a factor of h_∞/λ. As will become clear later in § 4,

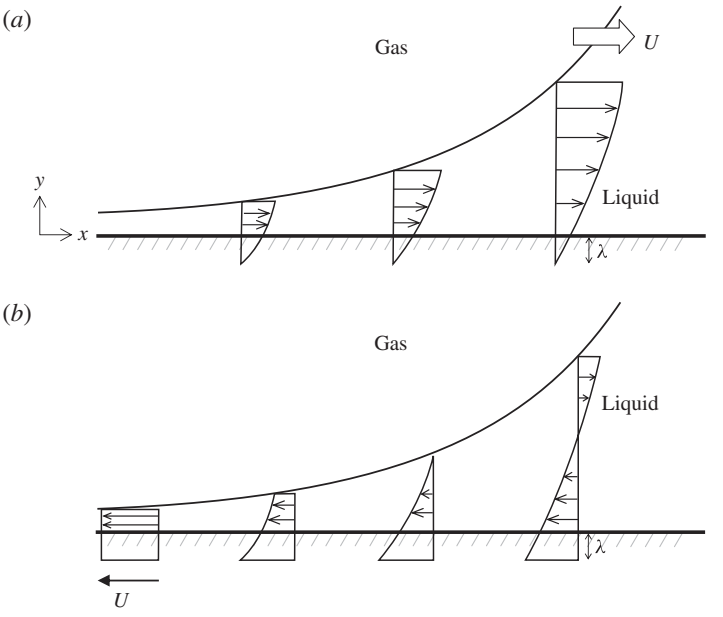

FIGURE 3. Flow mechanism for the Bretherton problem with slip walls. Here wall slip promotes capillary draining out of the film, and hence tends to make the film thickness thinner than in the no-slip case. (*a*) The fixed frame, (*b*) the frame moving with the bubble.

this additional factor h_∞/λ can actually be interpreted as a reduction of the apparent viscosity. Equation (2.9) also indicates that the apparent dynamic contact angle now varies like $\theta_d \approx h_\infty/\ell \propto Ca^{1/2}$, implying a different law for drop spreading on slippery surfaces. How this impacts drop spreading dynamics will be discussed in § 5.2.

Using $(h_\infty/\ell) \sim (h_\infty/R)^{1/2}$, (2.9) then leads to a new quadratic law for the film thickness:

$$\frac{h_\infty}{R} \sim Ca^2 \left(\frac{R}{\lambda}\right)^2. \tag{2.10}$$

Note that because $h_\infty < \lambda$, the above scalings only hold when Ca is below the breakdown point of the Bretherton law $Ca^* \sim (\lambda/R)^{3/2}$ (see also (2.11) below).

Compared to Bretherton's 2/3 law (2.6), the new scaling law (2.10) shows rather distinct ways in which h_∞ can vary with U, together with relevant length scales: (i) $h_\infty \propto U^2$ varies at a much faster rate than $U^{2/3}$; and (ii) instead of being linearly proportional to R, h_∞ varies like R^3/λ^2. More importantly, (2.10) crosses over Bretherton's 2/3 law at

$$Ca^* \sim \left(\frac{\lambda}{R}\right)^{3/2}, \tag{2.11}$$

which also marks the breakdown point of the Bretherton law at $h_\infty \sim \lambda$. It is clear that Ca^* must vanish as $\lambda \to 0$. The significance of this crossover is that it provides a critical bubble speed U^* below which the film can see slip effects by following the new quadratic law (2.10). It is worth emphasizing that although (2.11) is derived specifically for the Bretherton problem, a similar result can be found in dip coating

over textured surfaces (Seiwert *et al.* 2011, see also § 5.1) and forced dewetting on porous substrates (Devauchelle, Josserand & Zaleski 2007).

The new quadratic law (2.10) also modifies the dynamic pressure drop $\Delta p \sim (\sigma/R)(h_\infty/R)$ across the bubble:

$$\Delta p \sim \frac{\sigma}{R} Ca^2 \left(\frac{R}{\lambda}\right)^2. \tag{2.12}$$

Unlike the no-slip case, whose Δp varies like $1/R$ (see (2.7)), Δp here now grows linearly with R.

To sum up, (2.10) and (2.11) are the main results in this paper and indeed follow the respective scaling forms (2.2) and (2.3) postulated earlier. More importantly, they all involve λ, thus allowing us to relate these macroscopic quantities in terms of the amount of wall slip. Finally, we should point out that these new scaling results are derived from the standard lubrication approximation $p_x = \mu u_{yy}$, which holds only if $u_{yy} \gg u_{xx}$ (where the subscripts denote spatial derivatives in either the flow direction x or the transverse direction y). Because the transverse part scales at least as $u_{yy} \sim u_{cap}/h^2$ while $u_{xx} \sim (\lambda/h)u_{cap}/\ell^2$ can be best estimated from the plug flow on the lateral side, $u_{yy} \gg u_{xx}$ leads to the following criterion under which our analysis holds:

$$\lambda h/\ell^2 \ll 1 \quad \text{or} \quad \lambda/R \ll 1. \tag{2.13}$$

Below we carry out the formal lubrication analysis to calculate the film thickness h_∞ as a function of Ca and λ, as well as to test whether the results follow the new scalings derived above.

3. Lubrication theory

Following Bretherton's approach, we look at the transition region to derive the relevant lubrication equation for determining the film thickness. In a fixed frame, the fluid motion is governed by $\partial p/\partial x = \mu \partial^2 u/\partial y^2$ with the slip condition $u = \lambda \partial u/\partial y$ at the wall $y = 0$ and the free-stress condition $\partial u/\partial y = 0$ at the air–liquid interface $y = h(x)$. The velocity profile can be easily solved as

$$u = \frac{1}{2\mu}\frac{\partial p}{\partial x}(y^2 - 2h(y + \lambda)), \tag{3.1}$$

in which the pressure varies with $h(x)$ according to the linearized Young–Laplace equation at the interface:

$$p = -\sigma \frac{\partial^2 h}{\partial x^2}. \tag{3.2}$$

Integrating (3.1) over the film gives the flow rate (per unit width):

$$q = \frac{h^3}{3\mu}\left(1 + \frac{3\lambda}{h}\right)\left(-\frac{\partial p}{\partial x}\right). \tag{3.3}$$

Finally, fluid mass conservation requires q to be equal to the flow rate generated by the bubble's sweeping $U(h - h_\infty)$. This leads to the modified Bretherton equation

$$h^3 \frac{\partial^3 h}{\partial x^3}\left(1 + \frac{3\lambda}{h}\right) = 3Ca(h - h_\infty). \tag{3.4}$$

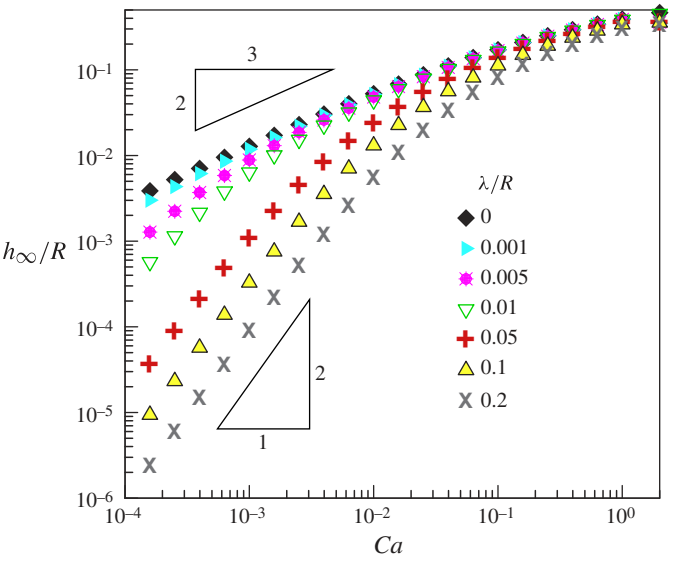

FIGURE 4. Dependence of the calculated film thickness h_∞/R on Ca for various values of λ/R. To better demonstrate effects of λ, the data are shown up to $Ca = 2$, although they are more appropriate for $Ca < 0.1$ because Ca is assumed small here. For small λ/R, the data closely follow the 2/3 power of Ca. Increasing λ/R makes the data deviate more from the 2/3 law, and the deviations become more apparent in the very small Ca regime where the data show $h_\infty/R \propto Ca^2$, as predicted by (2.10).

Boundary conditions are $h = h_\infty$, $\partial h/\partial x = 0$, $\partial^2 h/\partial x^2 = 0$ as $x \to -\infty$, and $\partial^2 h/\partial x^2 = 1/R$ as $x \to \infty$. The unknown h_∞ can be found by integrating the above equation numerically using the shooting method. Because a more accurate solution is needed to capture the transition between the no-slip limit and the strong slip limit, we take the arclength approach developed by Ratulowski & Chang (1989) to solve the problem. The detailed formulation and numerical procedures are given in appendix A.

Prior to showing our results, we remark that (3.3) and (3.4) reveal a number of characteristic differences between the no-slip limit and the strong slip limit. The scaling results found in the preceding section can also be formally justified. In the no-slip limit, (3.3) says $q \propto h^3$ and thus allows (3.4) to recover the Bretherton equation:

$$h^3 \frac{\partial^3 h}{\partial x^3} = 3Ca(h - h_\infty). \tag{3.5}$$

Balancing the terms on the two sides of this equation gives the cubic law (2.5) for the apparent dynamic contact angle. But in the strong slip limit, because of the factor λ/h increment in the flow rate, $q \propto h^2\lambda$, (3.4) ends up with a completely different equation:

$$h^2\lambda \frac{\partial^3 h}{\partial x^3} = Ca(h - h_\infty). \tag{3.6}$$

This gives a modified scaling relationship (2.9) for the apparent dynamic contact angle.

Figure 4 plots the calculated h_∞/R against Ca for various values of λ/R. It clearly shows that Bretherton's 2/3 law no longer holds in the range of $Ca(< 1)$. For a

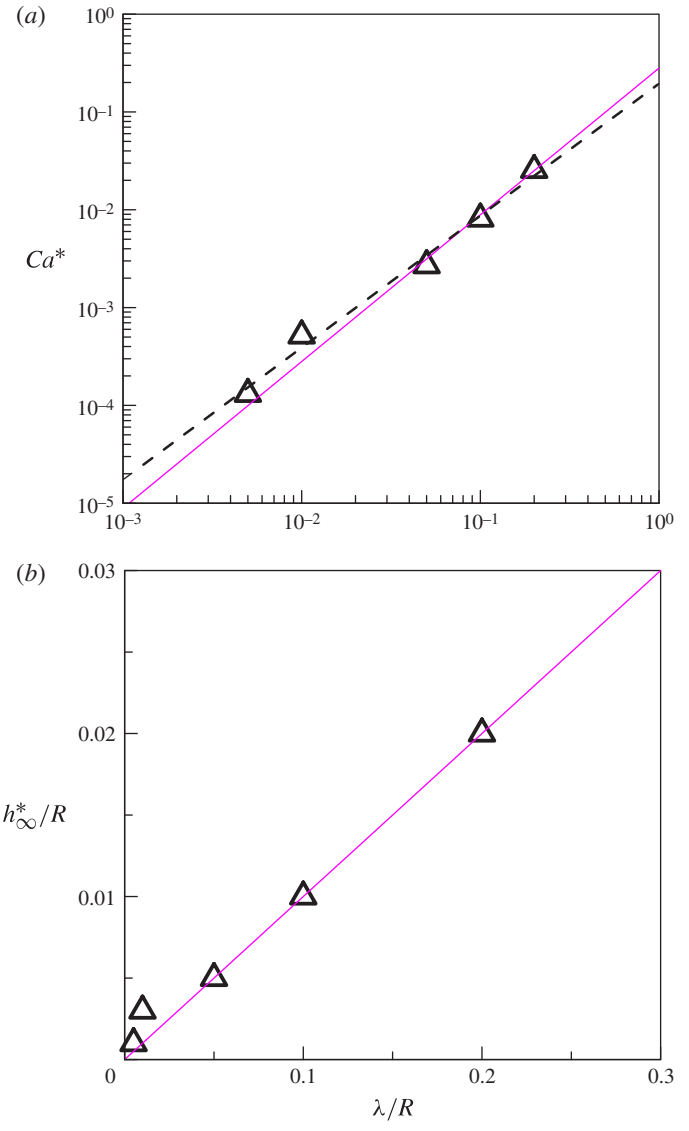

FIGURE 5. The critical capillary number Ca^* and the critical film thickness h^*_∞/R against λ/R at the breakdown point of the Bretherton law. For a given λ/R, the breakdown point is at the interception point formed by extrapolating the 2/3 law (from high to low Ca) and the quadratic law (from low to high Ca) in figure 4. In (a), the data can be captured by (2.11) according to $Ca^* = 0.281\ (\lambda/R)^{1.5}$ (solid line). The best fit curve (dashed line) $Ca^* = 0.195(\lambda/R)^{1.35}$ is also not far from the above. In (b), the data can be best described by $h^*_\infty = 0.10\lambda$, verifying $h_\infty \sim \lambda$ at the breakdown point of the Bretherton law.

given λ, the curve shows an apparent deviation from the 2/3 law for Ca below some critical value Ca^*. If Ca is sufficiently small, h_∞ scales like Ca^2 as predicted by (2.10). The transition from the 2/3 law to the quadratic law takes place at a larger Ca^* as λ is increased. Plotting Ca^* against λ/R in figure 5(a), we find that Ca^* exactly follows the 3/2 power of λ/R as predicted by (2.11). The corresponding critical film thickness

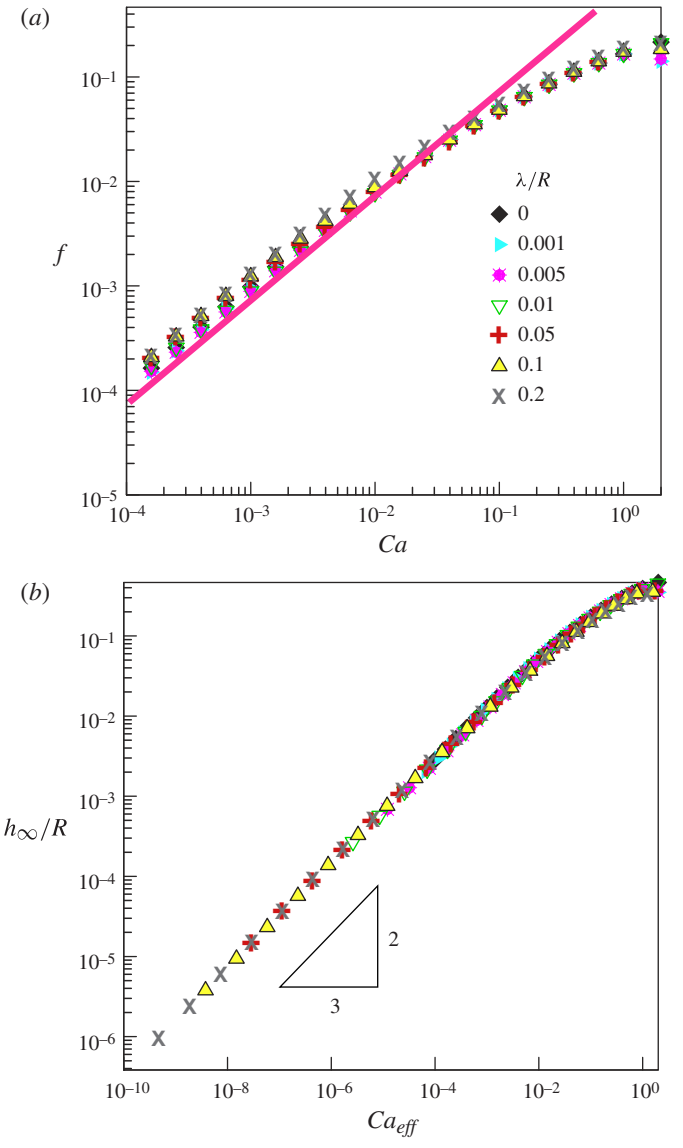

FIGURE 6. The data in figure 4 can be collapsed according to either (*a*) or (*b*). In (*a*), all the data for $Ca < 0.4$ can be best fitted by $f = 0.73Ca$ with $f = (h_\infty/R)^{3/2} + (h_\infty/R)^{1/2}(\lambda/R)$. In (*b*), much better data collapsing can be achieved in terms of the 2/3 power of the effective capillary number $Ca_{eff} = Ca\, h_\infty/(h_\infty + \lambda)$, with the viscosity μ replaced by the apparent viscosity $\mu h_\infty/(h_\infty + \lambda)$.

h^*_∞ is also plotted against λ in figure 5(*b*), showing $h^*_\infty = 0.1\lambda$ and hence verifying $h_\infty \sim \lambda$ at the breakdown point of the Bretherton law.

We also attempt to collapse the data and find that this can be done using a single master curve as shown in figure 6(*a*):

$$\left(\frac{h_\infty}{R}\right)^{3/2} + \left(\frac{\lambda}{R}\right)\left(\frac{h_\infty}{R}\right)^{1/2} = 1.37\ Ca. \tag{3.7a}$$

As is also shown in figure 6(*b*), it turns out that much better data collapse can be achieved by the alternative form of (3.7*a*):

$$\frac{h_\infty}{R} = 1.23\left(\frac{h_\infty}{\lambda + h_\infty}\right)^{2/3} Ca^{2/3}. \tag{3.7b}$$

This is essentially the Bretherton law (2.6) with μ replaced by $\mu h_\infty/(\lambda + h_\infty)$, which can be interpreted as the consequence of reduction in the apparent viscosity due to wall slippage. This effective 2/3 law appears to be universal, as will be shown later in § 4 when we extend the analysis to coating over structured/uneven surfaces.

The above findings have the following implications. When lowering the bubble speed U from high to low values under the small Ca condition, the film first shrinks like $U^{2/3}$ according to the Bretherton law. But this trend will no longer hold when U is lowered to the point where the film thickness is comparable to the slip length λ. As the film becomes thinner below λ by further decreasing U, it will undergo much more rapid thinning at the rate of U^2 due to much stronger capillary draining facilitated by wall slip. Because the bubble velocity at the transition point behaves like $U \propto (\lambda/R)^{3/2}$ from (2.11) and λ/R is typically small, one will need a very low U to see slip effects kick in. Also because $h_\infty \propto U^2$ from (2.10), the film in this case would become so thin that it would almost be in contact with the channel wall and hence susceptible to rupture. Our recent study has demonstrated that the film is indeed more vulnerable to rupture due to intensified capillary draining produced by wall slip (Liao *et al.* 2013). So the no-slip-to-slip transition here could be relevant to the wetting-to-dewetting transition seen in flows over structured hydrophobic surfaces (Sbragaglia *et al.* 2006) or the transition in gas–liquid slugs running from the hydrophilic section to the hydrophobic section in a composite microchannel (Oskooei & Sinton 2010).

4. Extension to textured surfaces: simple two-fluid models

It is well known that apparent slip can arise from surface roughness or structures (Lauga *et al.* 2007). Such slip often exists on uneven hydrophobic surfaces due to trapped vapour films or nanobubbles (Tyrrell & Attard 2001; Choi & Kim 2006; Ybert *et al.* 2007). In terms of wetting, because liquid tends to minimize its contact to such surfaces (Cassie & Baxter 1944), it is possible to create air pockets near the fluid–solid interface and hence apparent wall slippage (Quéré 2008). Note that it is generally difficult to completely wet hydrophobic surfaces. So to realize the Bretherton coating on such surfaces, it could be better achieved by having the walls pre-wetted by another fluid (e.g. Bico & Quéré 2002). In other words, the coating in this case can be thought to occur on a fluid surface, which can also produce apparent slip. A similar situation can also occur in spreading of polymer melts, in which large apparent slip can exist due to the less viscous layer near a surface (de Gennes 1979). De Gennes (1979) and Vinogradova (1995) introduced the concept of 'extrapolation length' to show that the apparent slip length can be much larger than the thickness of a thin film layer because of the abrupt reduction in viscosity near the surface.

Apparent slip can also occur for perfectly wettable, no-slip surfaces that have sizable pores or surface structures (Bonaccurso, Butt & Craig 2003). In this case, wetting liquid can penetrate into the interstitial spaces of a surface structure, shifting the effective slip plane into the liquid to resemble Beavers–Joseph-type slippage (Beavers & Joseph 1967). In terms of wetting, this favours decreasing the dynamic contact angle on a hydrophilic surface in that the surface energy can now be increased

by causing the wetting liquid to have more contacts with the surface (Wenzel 1936; Shirtcliffe *et al.* 2010).

So if a liquid film is deposited onto either type of textured surface, we anticipate that it should be thinner than that on a no-slip surface. Instead of using the more formal analysis to determine effective slip lengths (Feuillebois, Bazant & Vinogradova 2009; Belyaev & Vinogradova 2010; Asmolov & Vinogradova 2012), in appendix B we extend the extrapolation length approach of de Gennes and Vinogradova to derive the apparent slip length and viscosity for both textured hydrophobic and hydrophilic surfaces. To better illuminate the effects of apparent slip, we assume that whatever surface inhomogeneity arises from a textured surface can be somewhat coarse-grained or homogenized into an effective thin layer adjacent to the surface. With this homogenization, the averaged influence on flow due to surface structures can be represented by this layer with very distinct properties from the bulk. In other words, we use simple two-fluid models to capture the essential physics without looking at detailed surface microstructures. The results can then be used to elicit the features of the Bretherton coating for these surfaces.

We first consider the coating on a textured hydrophobic surface covered by a liquid film of thickness h. In this case, the averaged flow behaviour can be represented by a flow over a less viscous lubricating layer of thickness $\delta(\ll h)$ on the bottom, with viscosity μ_δ much lower than the bulk value μ. Under the constant pressure gradient condition, both the apparent slip length λ_{app} and viscosity μ_{app} (given respectively by (B 4) and (B 7)) are found to be

$$\lambda_{app} \approx \delta\left(\frac{\mu}{\mu_\delta} - 1\right), \tag{4.1a}$$

$$\mu_{app} \approx \left(\frac{h}{3\lambda_{app} + h}\right)\mu. \tag{4.1b}$$

Equation (4.1*a*) agrees with the result of Vinogradova (1995) and that of de Gennes (1979) when $\mu \gg \mu_\delta$.

For a similar film flowing over a textured hydrophilic surface, the bottom layer is now taken to be a porous one having permeability K_p that reflects fluid permeation effects in the interstitial spaces. The Darcy law is employed to model the flow within this layer, whose viscosity is taken to be the same as the bulk viscosity. The resulting apparent slip length and viscosity (given respectively by (B 10) and (B 12)) read as

$$\lambda_{app} \approx \frac{K_p}{h} - \delta, \tag{4.2a}$$

$$\mu_{app} \approx \left(\frac{h}{3\lambda_{app} + h}\right)\mu. \tag{4.2b}$$

Equation (4.2*a*) indicates that apparent slip can result if the permeability of the porous layer is sufficiently large in the sense that $K_p > \delta h$. It also suggests that as long as $K_p/\delta h > 2$, λ_{app} can be greater than the thickness of the porous layer, δ.

Although the apparent slip lengths (4.1*a*) and (4.2*a*) take different forms, they all reduce viscosity by the same factor of $h/(3\lambda_{app} + h)$ (wherein the factor 3 comes from the flow rate due to pressure forcing). Perhaps the simplest way to see this viscosity reduction can be derived from a simple shear flow over a slippery surface. By writing the bulk viscous stress $\mu V/h$ in terms of the apparent one $\mu_{app}V(\lambda_{app} + h)$ (with V being the shearing velocity), one can obtain a similar viscosity reduction ratio $\mu_{app}/\mu = h/(\lambda_{app} + h)$.

In any case, we can write $\mu_{app} = \mu h/(c\lambda_{app} + h)$ with c being a numerical factor. Replacing μ by μ_{app} above in the Bretherton law (2.6) gives

$$\frac{h_\infty}{R} \sim \left(\frac{h_\infty}{c\lambda_{app} + h_\infty}\right)^{2/3} Ca^{2/3}. \tag{4.3}$$

This is essentially (3.7*b*) (by taking $c = 1$ in (4.3)). Obviously, for both $\lambda_{app} \ll h_\infty$ and $\lambda_{app} \gg h_\infty$, (4.3) recovers Bretherton's 2/3 law and the quadratic law (2.10), respectively. Hence, it allows us to capture the transition between these two laws in a unified manner. This also explains why (3.7) can successfully collapse the data in the entire range of $Ca < 1$ in figure 6. We also find that data collapse here is not sensitive to the value of c chosen (as long as $c = O(1)$). As such, the effective 2/3 law (4.3) can be considered universal. Therefore, all the new scalings found in § 3 should be equally applicable to textured surfaces.

It is worth mentioning that (4.3) can also be applied to the situation where the apparent slip length λ_{app} becomes *negative*. This can happen either to (4.1*a*) with $\mu_\delta > \mu$ when the surface layer is more viscous than the bulk, or to (4.2*a*) with $K_p < \delta h$ when the porous layer is less permeable. In general, this negative slip occurs on a no-slip, uneven surface of small undulation amplitude ε when one would like to derive the effective boundary condition on the averaged plane of the surface. Specifically, the effective boundary condition can be derived by taking a Taylor expansion around the plane $y = 0$, i.e. $u(y = \varepsilon) \approx u(y = 0) + \varepsilon \partial u/\partial y|_{y=0} + \cdots = 0$, giving $u(y = 0) \approx \lambda_{app} \partial u/\partial y|_{y=0}$ with $\lambda_{app} = -\varepsilon < 0$. Note that the above derivation is more applicable for $h_\infty \gg \varepsilon$. So for coating on such a surface, because $\mu_{app} = \mu/(1 - c\varepsilon/h_\infty)$ is now greater than the bulk value, the deposited film thickness h_∞ given by (4.3) will be thicker than the Bretherton law by a factor of $(1 - c\varepsilon/h_\infty)^{-2/3}$. That is,

$$\frac{h_\infty}{R} \sim \left(\frac{1}{1 - c\varepsilon/h_\infty}\right)^{2/3} Ca^{2/3}. \tag{4.4}$$

This thickening effect would become gradually stronger as h_∞ is decreased by lowering Ca, which might explain slightly thicker films seen in the experiment by Krechetnikov & Homsy (2005). Equation (4.4) also indicates that its validity can only hold before h_∞ reaches $O(\varepsilon)$. Hence, it starts to break down when Ca is around the critical value $Ca^* \sim (\varepsilon/R)^{3/2}$, similar to (2.11). For $Ca < Ca^*$, the film thickness can only be $O(\varepsilon)$ as the liquid has to fill into the grooves of the surface before forming a continuously wetting film.

5. Connections to dip coating and drop spreading

To the best of our knowledge, we have not seen any Bretherton-type experiment that allows us to make direct comparison with our theoretical predictions. Perhaps this can be carried out by displacing a liquid with a gas bubble in a hydrophobic microchannel like the experiment by Oskooei & Sinton (2010), or by applying a similar setup to generate a large apparent slip by depositing a liquid film onto the channel wall pre-wetted by another immiscible fluid layer (e.g. Bico & Quéré 2002).

Despite the lack of direct experimental evidence to support our theory, there exist two closely related problems, dip coating and drop spreading, which are known to share common features with the Bretherton problem (de Gennes *et al.* 2003; Stone 2010; Liao *et al.* 2013) and provide many experiments with which we can

make comparisons. So it might be more desirable to make connections with these two problems in order to take a broader look at the role played by wall slip. We emphasize that here we do not use such connections as a rigorous test of our theory by making quantitative comparison with experiments. Rather, such connections are made qualitatively in a scaling sense. As we will demonstrate below, this approach not only provides a more lucid way to look at how wall slip modifies interfacial flow characteristics but also offers plausible accounts for apparent departures from no-slip predictions seen in experiments. More importantly, this might provide feasible alternatives to assessing wall slip effects experimentally.

5.1. *Dip coating over structured/uneven surfaces*

The connection to dip coating is obvious, as it belongs to the same class as Landau–Levich–Bretherton flow. Seiwert *et al.* (2011) performed dip coating over a plate textured with micropillars. In their experiment, the coating is carried out by pulling the plate from a bath of liquid in the range $10^{-4} < Ca < 10^{-2}$, where Ca is based on the withdrawal velocity V. At high V, the deposited film thickness h_d is found to increase with V such that it approximately follows the Bretherton law (wherein R is taken as the capillary length $(\sigma/\rho g)^{1/2} \sim 1$ mm with ρ being the fluid density and g the gravitational acceleration). At low V, on the other hand, h_d is thickened by strong viscous dissipation imparted by the pillars and tends to approach the pillar height h_p independent of V. As discussed at the end of § 4, the pillar height here in fact acts like a negative slip length, tending to thicken the film according to (4.4). It also marks the point around which (4.4) starts to break down when h_d is close to h_p. The critical capillary number found in their study is $Ca^* \sim (h_p/R)^{3/2}$, which is exactly the breakdown point of (4.4).

In a related study, Krechetnikov & Homsy (2005) found in their experiment on dip coating over roughened substrates that the measured film thickness for $Ca = 10^{-4}$–10^{-2} is slightly thicker than Bretherton's 2/3 law such that the deviations become diminished as the film gets thicker at larger Ca. The observed film thickening seems to roughly follow (4.4) and, again, can be interpreted in terms of negative slip length.

5.2. *Drop spreading*

Concerning drop spreading, its connection to the Bretherton problem is rooted in the fact that the flow in the transition region of the Bretherton problem can be used to describe the outer wedge flow away from the contact line: both simply involve the balance between surface tension and viscous forces from a purely macroscopic viewpoint (de Gennes *et al.* 2003; Stone 2010; Liao *et al.* 2013). Because of this, the apparent dynamic angle relationship in the Bretherton problem can be used to derive wetting and spreading laws in drop spreading (Stone 2010; Liao *et al.* 2013) without having to include detailed molecular wetting effects in the inner precursor film region (Kalliadasis & Chang 1996).

Perhaps a better way to see how the Bretherton problem is connected to drop spreading is to look at the outer film equation in the latter (in the frame moving with the contact line) under the perfectly wetting condition (Eggers 2004)

$$3Ca\, h = -(h^3 + 3\lambda h^2)h_{xxx}, \tag{5.1}$$

where the subscripts indicate the derivatives with respect to x. One can clearly see that (5.1) is identical to (3.4) with $h_\infty = 0$. At $\lambda = 0$, a simple balance between $Ca\, h$ and $h^3 h_{xxx}$ immediately leads to the well-known Hoffman–Tanner law $\theta_d = h_x \sim h/\ell \sim Ca^{1/3}$

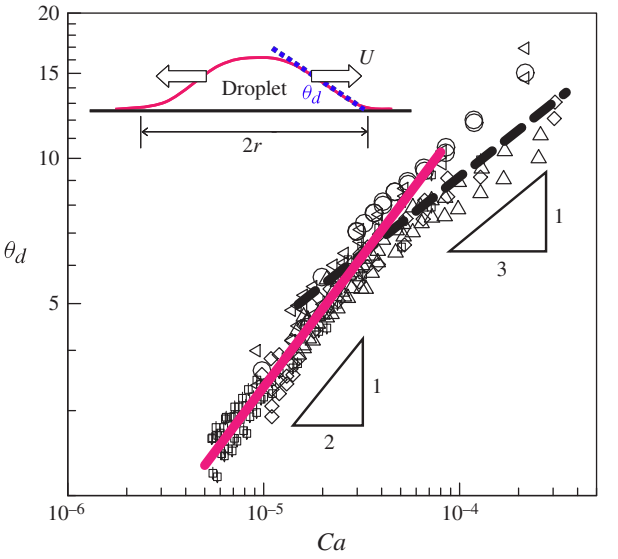

FIGURE 7. Apparent dynamic contact angle data (symbols) found in the drop spreading experiment by Chen (1988). For $Ca > 3 \times 10^{-5}$, the data can be roughly fitted by $\theta_d = 201.3Ca^{0.33}$ (long-dashed line) in accordance with the no-slip Hoffman–Tanner law $\theta_d \sim Ca^{1/3}$. For $Ca < 3 \times 10^{-5}$, however, the data can be best described by $\theta_d = 1674.3Ca^{0.54}$ (pink solid line), as predicted by $\theta_d \propto Ca^{1/2}$ according to (5.2). The apparent departure from the Hoffman–Tanner law can be attributed to large apparent wall slip existing in the polydimethylsiloxane (PDMS) liquid used in Chen's experiment.

for the apparent dynamic contact angle, identical to (2.5) obtained from the Bretherton problem (Kalliadasis & Chang 1994, 1996; Stone 2010). It is worth mentioning that the Hoffman–Tanner law can also be derived using the local viscocapillary energy argument of de Gennes for the wedge flow near the contact line (de Gennes 1985). Therefore, we believe that our new scaling results for the Bretherton problem should enable us to elicit some physics in drop spreading on slippery surfaces, especially under the perfect wetting condition or for the spreading of a droplet over a pre-existing film.

Having the outer film equation (5.1) in connection to the Bretherton problem, we find that some drop spreading experiments can be interpreted in terms of wall slip. Chen (1988) conducted a drop spreading experiment on glass substrates and measured how the apparent dynamic angle θ_d varies with Ca. In his experiment, the fluid is silicone oil made of polydimethylsiloxane (PDMS), a typical polymeric liquid that can impart a large apparent slip (de Gennes 1979). According to Brochard-Wyart *et al.* (1994), the apparent slip length for such a liquid can be estimated as $\lambda \sim a_m N^3/N_e^2$, strongly depending on the number of polymerization, N, and the degree of chain entanglement N_e, where a_m is the monomer size of ~0.1 nm. For $N \sim 10^3$ used in Chen's experiment and $N_e \sim 10^2$, λ can be as large as 10 μm.

With the above in mind, let us take a look at Chen's data shown in figure 7. For $Ca > 3 \times 10^{-5}$ his data roughly follow the Hoffman–Tanner law $\theta_d \sim Ca^{1/3}$, as is commonly seen in drop spreading on no-slip surfaces. For $Ca < 3 \times 10^{-5}$, however, the data show a systematic departure from the Hoffman–Tanner law. We find that θ_d in this regime actually exhibits much stronger dependence on Ca: $\theta_d \propto Ca^{1/2}$. In fact,

this 1/2 law can be obtained using (5.1) with $h \ll \lambda$ (or (2.9)) by setting $\theta_d \sim h/\ell$ to be the ratio of the drop height h to the spreading radius r:

$$\theta_d \sim Ca^{1/2}(r/\lambda)^{1/2}. \tag{5.2}$$

Equation (5.2) is also consistent with the result using the local energy dissipation argument of de Gennes, in which the surface tension energy $\sigma\theta_d^2 U$ is balanced to the viscous dissipation energy $\mu U^2 r/\lambda$, similar to what he did for liquid spreading on no-slip substrates (de Gennes 1985). The successful capture of Chen's data by the 1/2 law in the very small Ca regime strongly implies the existence of wall slip in his experiment.

It should be pointed out that in most drop spreading experiments, a droplet usually starts with its height h much greater than λ. So for short times, its spreading behaviour should still follow the Hoffman–Tanner 1/3 law until $h \sim \lambda$. If the droplet can keep spreading after this point, the slightly greater 1/2 law should govern the long-term spreading behaviour. In other words, a no-slip-to-slip transition should occur during the spreading, which is exactly what Chen's data display. Because θ_d given by (5.2) has be to be smaller than $\theta_d \sim Ca^{1/3}$ for the no-slip case, slip effects would become important for $Ca < Ca' \sim (\lambda/r)^3$. Given that the data start to depart from the Hoffman–Tanner law at $Ca \approx 3 \times 10^{-5}$, we can set this Ca to be Ca' to estimate the slip length as $\lambda \sim 10^{-2} r$. For $r \sim 1$ mm used in his experiments, λ is of the order of 10 μm. It is not only comparable to the film thickness in the late stage of the spreading seen in his experiments, but also in agreement with the value estimated earlier based on the report by Brochard-Wyart *et al.* (1994).

In terms of spreading dynamics, (5.2) also implies a new spreading law governing how the drop spreading radius r grows with time t, which can be derived from (5.2) by writing the spreading speed $U \sim r/t$ under the constant volume constraint $\Omega \approx (\Pi/2)hr^2 \sim \theta_d r^3$:

$$r \sim (t\Omega^2 \lambda\sigma/\mu)^{1/8}. \tag{5.3}$$

This 1/8 law was first reported by Brochard & de Gennes (1984) for spreading of polymeric droplets. As expected, the spreading is faster than the classical Tanner 1/10 law $r \sim (t\Omega^3\sigma/\mu)^{1/10}$ (as a direct consequence of the Hoffman–Tanner law $\theta_d \sim Ca^{1/3}$) for the no-slip case (Tanner 1979). It is worth mentioning that a similar 1/8 law can occur in gravity-driven spreading (Lopez, Miller & Ruckenstein 1976), which is more appropriate for large droplets. So if a small drop is used and its spreading is found to obey Tanner's 1/10 law followed by the new 1/8 law (5.3), this might imply the existence of wall slip on the surface. The no-slip-to-slip transition should also occur at the crossover time between these two spreading laws:

$$t^* \sim (\Omega^2/\lambda^5)(\sigma/\mu)^{-1}. \tag{5.4}$$

Since it decays very rapidly, like λ^{-5}, if λ is too small, the time required to see this transition would be prohibitively long. This explains why Tanner's law is always observed in most of the drop spreading experiments. In contrast, if (5.3) or (5.4) can be observed, wall slip effects might no longer be negligible. In fact, we do find such experimental evidence. Similar to Chen (1988), Albrecht, Otto & Leiderer (1992) also employed PDMS liquid to conduct their drop spreading experiment. In their study, the liquid has a much lower molecular weight. So the slip length might be smaller than that in Chen's study. However, the droplets they used are picolitre-sized, with radius $r \sim 1$ mm and much smaller thickness $h \sim 10$ nm. Since the latter could be smaller

than the slip length, the spreading might be dominated by slip effects. Indeed, their data do show $r \sim t^{0.13}$, close to $r \sim t^{0.125}$ predicted by (5.3).

6. Connection between slip length and molecular length, and their coupling

The connection to drop spreading we made above is based on the hydrodynamic resemblance between the outer wedge flow and Bretherton film flow at the macroscopic level. In the inner region, where the stress singularity becomes inevitable when approaching the contact line, one often either introduces an additional slip length or molecular disjoining pressure effects to relieve the contact line singularity (Bonn *et al.* 2009). Since one can also produce some sort of cutoff length to prevent the blowing up of the contact-line force, this implies that, at the micro/mesoscopic level, the slip length might be somewhat connected to the molecular length created by disjoining pressure. So in this section, we will look more into this connection. In addition, to link to the outer film flow described by (5.1), we will also look at how these two effects intervene to modify the film structure in the inner region near the contact line.

We begin with the work of Denkov *et al.* (2005), who studied the wall slip phenomenon in foams or concentrated emulsions. They considered the sliding motion of foam bubbles over a no-slip wall and determined the wall friction force F_w as a function of the bubble sliding velocity U under a constant pressure forcing ΔP. Because there is a wetting film between the bubbles and the wall, the slip effect here can be said to be an apparent one. By assuming that most of the viscous dissipation is concentrated on the film, these authors showed that if bubble surfaces are tangentially immobile, F_w is found to vary like $U^{1/2}$, as opposed to $F_w \propto U$ commonly seen in viscous flows. This result also differs from $F_w \propto U^{2/3}$ based on the Bretherton law for mobile bubble surfaces. Their result $F_w \propto U^{1/2}$ actually arises from the fact that the viscous shearing essentially takes place over the entire film (of length L). Since the film thickness scales as $h \sim (\mu UL/\Delta P)^{1/2} \propto U^{1/2}$ using a simple force balance, this gives the wall viscous stress $\tau_w \sim \mu U/h \propto U^{1/2}$ and hence $F_w \propto U^{1/2}$. But if wall slip is included and the effects are assumed to be strong ($\lambda \gg h$), the wall viscous stress will turn to $\tau_w \sim \mu U/\lambda \propto U$, independent of h which scales as $\mu UL/(\Delta P\lambda)$ using $\Delta Ph \sim \tau_w L$. Therefore, the dependence of τ_w on U will change from $U^{1/2}$ to U when no-slip turns to strong slip. This transition again occurs at $h \sim \lambda$, corresponding to $U \sim \Delta P\lambda^2/\mu L$.

In a related work, Saugey, Drenckhan & Weaire (2006) reconsidered the problem of Denkov *et al.*, but allowed bubble surfaces to be fully mobile. Further, taking disjoining pressure into account, they found in their simulations that F_w can vary with U (via Ca) in different powers ranging from 0.5 to 1. Specifically, $F_w \propto U$ for low U whereas $F_w \propto U^n$ with $n = 0.5$–0.6 for large U (but still in the small Ca regime). It is somewhat surprising that this power law change is similar to that for the immobile bubble case when no-slip turns to strong slip, implying that disjoining pressure might produce effects similar to wall slip.

Indeed, as disjoining pressure tends to thicken films and hence to reduce viscous drag, it does produce effects similar to wall slip. This pressure is often written as $\Pi = \sigma a^2/h^3$ characterized by the molecular length $a = (A/6\pi\sigma)^{1/2} \sim 1$ Å, where A is the Hamaker constant of the order of 10^{-20}–10^{-19} J (de Gennes 1985). The connection between disjoining pressure and wall slip can be seen by considering a film flow at a quasi-static state where disjoining pressure is balanced to the Laplace pressure $\sim\sigma/R$ (arising from the bubble meniscus). The resulting film thickness scales

as $h_1 \sim R(a/R)^{2/3}$ and hence the wall stress $\tau_w \sim \mu U/h_1 \sim \mu U/(a^2R)^{1/3}$. Compared to $\tau_w \sim \mu U/\lambda$ for the strong slip situation, the effects produced by disjoining pressure are essentially equivalent to those by the slip length $\lambda \sim (a^2R)^{1/3}$. This equivalence can also be established by setting the crossover capillary number with wall slip, $Ca^* \sim (\lambda/R)^{3/2}$ (i.e. (2.11)), to be equal to the capillary number $Ca_1 \sim a/R$ corresponding to $h_1 \sim R\,Ca^{2/3}$ when the Bretherton 2/3 law ceases to hold (Teletzke, Davis & Scriven 1988). A similar equivalence can also be found in the context of dynamic wetting, showing that both wall slip and disjoining pressure (in the precursor film) give a virtually identical logarithmic correction to the dynamic contact angle relationship in relieving the contact line stress singularity (Kalliadasis & Chang 1996; Yeo & Chang 2006; Savva & Kalliadasis 2011).

We should remark that the usual equivalence between wall slip and disjoining pressure can only be established by comparing their effects when each exists alone. In common drop spreading problems, either wall slip or disjoining pressure merely manifests locally near the contact line — both are unimportant in the bulk away from the contact line. However, if slip effects prevail throughout a spreading drop whose height is within the slip length, the precursor film might have a structure rather different to the usual one, since both slip and disjoining pressure effects are now coupled. The situation here might be relevant to the spreading of a small polymeric drop whose apparent slip length could be large (Brochard-Wyart *et al.* 1994).

Based on the above reasoning, it would be interesting to see how both wall slip and disjoining pressure together determine the structure of the precursor film under the strong slip condition. The common approach to a problem of this sort involves three steps: (i) solve the outer macroscopic flow away from the contact line, which is exactly governed by the Bretherton-type equation (see (5.1)); (ii) solve the inner flow problem for the precursor film; and (iii) match the solutions of (i) and (ii), which yields the dynamic contact angle relationship (Kalliadasis & Chang 1994). Here we do not intend to solve the entire problem, which is beyond the scope of this paper. Instead, we follow the spirit of matched asymptotics to elicit qualitative features of the precursor film in connection with our results given in §§ 2 and 3.

It is more convenient to work on the problem in the frame moving with the contact line. Similar to (5.1), we begin with the equation $p_x(h^3 + 3\lambda h^2) = 3\mu Uh$, where the pressure is modified as $p = -\sigma h_{xx} - \Pi(h) = -\sigma h_{xx} - \sigma a^2/h^3$ (Bonn *et al.* 2009) by including disjoining pressure in terms of the molecular length $a = (A/6\pi\sigma)^{1/2}$. When slip effects prevail (i.e. $\lambda \gg h$), the equation can be reduced to $p_x\lambda h^2 = \mu Uh$, giving

$$Ca\, h = -\lambda h^2 h_{xxx} + 3a^2\lambda h_x/h^2. \tag{6.1}$$

To the best of our knowledge, (6.1) is the first equation that takes into account both wall slip and disjoining pressure effects in determining the precursor film structure, as derived in our recent report (Liao *et al.* 2013). As is also demonstrated in the same report, several features below can be obtained in the scaling sense from this equation, and these are worth reiterating here. For the macroscopic flow, the disjoining pressure term is negligible, and hence (6.1) recovers a form similar to (3.6). So the balance between the capillary term $\lambda h^2 h_{xxx}$ and the viscous term $Ca\, h$ in (6.1) yields the apparent dynamic angle relationship (2.9). The same balance in the inner precursor film region is equivalent to matching the macroscopic contact angle θ_d to the microscopic one, providing a connection between the characteristic thickness h_f and length ℓ_f for the precursor film,

$$(h_f/\ell_f)^2 \sim Ca(\ell_f/\lambda). \tag{6.2}$$

Balancing the viscous term and the disjoining pressure term provides an additional relationship between h_f and ℓ_f,

$$(a/h_f)^2 \sim Ca(\ell_f/\lambda), \tag{6.3}$$

or $h_f \sim (a\ell_f)^{1/2}$ by eliminating Ca because of (6.2). Combining (6.2) and (6.3), the thickness and length of the precursor film are found to be

$$h_f \sim a(\lambda/a)^{1/4}Ca^{-1/4} \quad \text{and} \quad \ell_f \sim a(\lambda/a)^{1/2}Ca^{-1/2}. \tag{6.4a,b}$$

These results are quite different from $h_f \sim a\,Ca^{-1/3}$ and $\ell_f \sim a\,Ca^{-2/3}$ for liquid spreading over a no-slip surface (Hervet & de Gennes 1984; Kalliadasis & Chang 1996; Eggers & Stone 2004). Also compared to the above no-slip scalings, both h_f and ℓ_f predicted by (6.4) can be greater if λ is sufficiently large such that $(\lambda/a)^3Ca > 1$. Such large wall slip might occur in spreading of polymeric liquids. For instance, for $\lambda \sim 1$ μm, $a \sim 1$ Å, and $Ca \sim 10^{-5}$, the estimated film dimensions are $h_f \sim 20$ nm and $\ell_f \sim 3$ μm, which might be detectable in experiments. Moreover, because $\ell_f \propto Ca^{-1/2} \propto (\ell_f/t)^{-1/2}$ from (6.4*b*), the film will spread like $\ell_f \propto t^{1/3}$ in an anomalous diffusion manner, in contrast to $\ell_f \propto t^{1/2}$ for diffusive films commonly observed in experiments (Heslot, Cazabat & Levinson 1989; Xu *et al.* 2004). Note that in the no-slip case, $\ell_f \sim a/Ca^{2/3}$ leads the precursor film to spread like $\ell_f \propto t^{2/5}$, which is not diffusive either. In the recent experimental study by Mate (2012) on spreading of polymeric droplets, the measured spreading exponent is found to range between 0.31 and 0.42, fairly close to the 1/3 law at the strong slip state and the 2/5 law at the no-slip state, respectively. So the transition between these two distinct spreading dynamics can be interpreted as a consequence of the no-slip-to-slip transition.

Given (6.4) as well as the experimental support by Mate (2012), a new precursor film structure might actually exist due to combined effects of wall slip and disjoining pressure. Also guided by (6.4), one can then apply the matched asymptotic techniques to determine the detailed precursor film structure and hence amend (5.2) to give a full account of how θ_d depends on a, λ, r, and Ca. These tasks will be left to a future study.

7. Concluding remarks

We have demonstrated that the features of the Bretherton problem can be significantly modified by wall slip effects. A slippery wall is somewhat similar to a free surface in the sense that a fluid can run with less viscous resistance. But the difference here is that the residual viscous stress on the wall in the former can impart an additional slip length λ to change flow characteristics qualitatively. This is manifested by the fact that flow resistance at the strong slip state varies like h^{-2}, as opposed to h^{-3} in the usual no-slip case. Because of this, the presence of wall slip can lead to the following changes to the Bretherton problem.

(i) Bretherton's 2/3 law $h_\infty \sim R\,Ca^{2/3}$ breaks down at $Ca^* \sim (\lambda/R)^{3/2}$, below which a new quadratic law $h_\infty \sim R\,Ca^2(R/\lambda)^2$ emerges to govern the behaviour of film thickness smaller than λ. The film in this strong slip regime also becomes much thinner than that predicted by the 2/3 law for the no-slip case.

(ii) Both the 2/3 and the quadratic laws can be unified as $h_\infty/R \sim Ca^2R^2/(\lambda + h_\infty)^2$. This universal coating law can be re-expressed as the effective 2/3 law, $h_\infty/R \sim Ca_{eff}^{2/3}$, with the viscosity μ replaced by the apparent viscosity $\mu_{app} = \mu h_\infty/(\lambda + h_\infty)$ in $Ca_{eff} = \mu_{app}U/\sigma$. Since a similar viscosity reduction factor can occur in

coating over textured surfaces whose apparent slip lengths could be large, our findings should also be applicable to such surfaces.

The above results also imply that even a fraction of wall slip can have profound effects on the Bretherton problem. To better illustrate this point, we consider a bubble displacement in a microchannel of $R \sim 100$ μm. Assume the slip length to be $\lambda \sim 1$ μm, which is merely 1 % of the channel depth. So the Bretherton law only holds for $Ca > Ca^* \sim (\lambda/R)^{3/2} \sim 10^{-3}$. But for $Ca < Ca^*$, the film thickness is described by the quadratic law $h_\infty \sim R\,Ca^2(R/\lambda)^2$. For $Ca \sim 10^{-4}$, this gives $h_\infty \sim 10^{-4}R \sim 10$ nm. The Bretherton law with the same Ca gives $h_\infty \sim R\,Ca^{2/3} \sim 0.02R \sim 2$ μm. So the film thickness on slip walls is thinner by two orders of magnitude compared to that without slip. Given that the amount of slip here is merely 1 % of the channel depth, the impact is quite remarkable. In other words, the coating will be very sensitive to the amount of wall slip. If the coating speed is not sufficiently high to make the film much thicker than the slip length, more rapid thinning can occur in the film, making it more vulnerable to rupture.

To gain more insights into the role played by wall slip, we also make connections to both dip coating and drop spreading. For drop spreading, in particular, the quadratic law from the Bretherton problem implies a new 1/2 law for the apparent dynamic contact angle, $\theta_d \propto Ca^{1/2}$ (see (5.2)). This not only successfully captures the experimental data reported by Chen (1988) but also explains why his data in the small Ca regime show an apparent departure from the classical Hoffman–Tanner law, $\theta_d \sim Ca^{1/3}$. The success in capturing Chen's data thus provides indirect evidence supporting our results for the Bretherton problem. An immediate consequence of this new wetting law is that, instead of Tanner's 1/10 law, the spreading radius can grow with time at a slightly faster rate of $r \propto t^{1/8}$, which is close to the experimental observation by Albrecht *et al.* (1992). At the microscopic level, we suggest a new precursor film structure described by (6.4) due to the combined effects of wall slip and disjoining pressure. This leads to the anomalous 1/3 diffusion law governing the spreading dynamics of the film, which is observed in the recent experimental study by Mate (2012). We emphasize that all these experiments are carried out using polymeric liquids whose apparent slip lengths can be large. So it is likely that the apparent departures from the no-slip scalings seen in these experiments can be attributed to strong wall effects.

Since all these findings are very sensitive to the amount of wall slip, it might be advantageous to apply them to quantify slip effects. For instance, if one would like to measure the slip length for a surface, one can apply the Bretherton-type bubble displacement or the Landau–Levich-type coating to look at how the film thickness varies with the coating speed and how the result deviates from Bretherton's 2/3 law. In particular, the critical capillary number $Ca^* \sim (\lambda/R)^{3/2}$, at which the 2/3 law turns to the quadratic law, can be used to determine the amount of slip. For a planar surface, perhaps the simplest way to identify whether wall slip exists is to place a tiny droplet on it. By observing how the droplet spreads with time and looking at whether there is any transition from the 1/10 law to the 1/8 law, one might be able to estimate the slip length of the surface. Because all these approaches utilize distinctive no-slip-to-slip transitions, they should be more accurate than conventional surface force apparatus in determining the amount of slip experimentally.

Our findings can also be useful in coating and microfluidic applications. In coating, there is often the need to deposit thin layers on chemically decorated or textured surfaces. If the slip length is known, one can always apply the effective 2/3 law (3.7*b*)

to control the deposited film thickness. As for microfluidic applications, the same law can be used to control the formation of wetting films in gas–liquid slug flows.

Acknowledgement

This work is supported by the National Science Council of Taiwan under grant 101-2221-E-006-230-MY3 to H.H.W.

Appendix A. Arclength approach to solving (3.4) numerically

This appendix describes how to implement the arclength approach of Ratulowski & Chang (1989) to solving (3.4), to determine the film thickness h_∞ numerically. It is an approach that enables us to determine h_∞ directly without having to assume its scaling, as was done by Bretherton (1961) in his analysis. More importantly, as shown by Ratulowski & Chang (1989) for the no-slip case, not only is this approach more accurate than Bretherton's, but also the calculated film thickness is found to be in excellent agreement with that from direct numerical simulations (Reinelt & Saffman 1985) up to $Ca = O(10^{-1})$.

Now consider the motion of a long bubble in a slit-like channel of depth $2b$. We non-dimensionalize the problem by rescaling length, velocity, and time with b, σ/μ, and $b\mu/\sigma$, respectively. Since the bubble moves at a constant dimensionless velocity Ca, we solve the problem in a moving frame, $\zeta = x - Ca\, t$. Because of fluid mass conservation, the flow rate within the film q_f in the stationary frame reads

$$q_f(r, r_0) = Ca(r - r_0), \tag{A 1}$$

where r is the distance from the centreline of the channel to the air–liquid interface and becomes a constant r_0 in the flat part of the bubble. From lubrication theory, q_f can be related to the Laplace pressure (3.2) on the air–liquid interface according to

$$q_f = -K\,\frac{\mathrm{d}p}{\mathrm{d}\zeta}, \tag{A 2}$$

with the mobility coefficient K given by

$$K(r) = \frac{\eta^3}{3}\left(1 + \frac{3\Lambda}{\eta}\right), \tag{A 3}$$

where $\eta = 1 - r$ is the dimensionless film thickness and $\Lambda = \lambda/b$ is the ratio of the slip length to b. For no-slip surfaces ($\Lambda = 0$), (A 3) reduces to $K = \eta^3/3$, as used in the study by Ratulowski & Chang (1989).

Writing the force balance along the bubble in terms of the arclength variable s pointing toward the front of the bubble, we solve the following set of equations for determining the bubble shape:

$$\frac{\mathrm{d}\zeta}{\mathrm{d}s} = \cos\theta, \tag{A 4a}$$

$$\frac{\mathrm{d}r}{\mathrm{d}s} = -\sin\theta, \tag{A 4b}$$

$$\frac{\mathrm{d}r}{\mathrm{d}s} = -\frac{\cos\theta}{K(r)}q_f(r, r_0), \tag{A 4c}$$

$$\frac{\mathrm{d}\theta}{\mathrm{d}s} = -p, \tag{A 4d}$$

where θ is the tangential angle at a given point along the bubble surface. We integrate these equations by starting from the flat portion of the bubble where a unique fixed point exists (Ratulowski & Chang 1989). The initial conditions for this numerical integration are

$$\zeta = 0, \quad r = r_0, \quad p = 0, \quad \theta = 0. \tag{A 5}$$

Because the film thickness $1 - r_0$ is unknown, we guess a value for r_0 and integrate (A 4) with (A 5) using the fourth-order predictor–corrector method to determine the interface profile. The value of r_0 is then corrected using the symmetric condition at the bubble tip:

$$\theta = \pi/2, \quad r = 0. \tag{A 6}$$

At a given Ca, we employ the Newton–Raphson method to find r_0 iteratively until (A 4)–(A 6) are satisfied completely.

Appendix B. Simple two-fluid models for flows past textured surfaces

Extending the extrapolation length approach by de Gennes (1979), Vinogradova (1995), we employ simple two-fluid models to determine the apparent slip length and viscosity for flows past textured surfaces. A liquid film of thickness h consists of a bulk free layer of viscosity μ and a much thinner lubricating layer of thickness δ ($\ll h$) on the bottom wall. The lubricating layer can be either fluid or a porous medium. Let $u(y)(\delta \leqslant y \leqslant h)$ and $u_\delta(y)(0 \leqslant y \leqslant \delta)$ denote the velocity profiles for the bulk free layer and the lubricating layer, respectively. The entire film is subjected to a constant pressure gradient $-\mathrm{d}P/\mathrm{d}x \equiv G > 0$.

B.1. *Textured hydrophobic surface*

To model an interfacial flow past a textured hydrophobic surface, the lubricating layer has viscosity μ_δ much lower than the bulk value μ. The top surface $y = h$ is stress-free: $\mathrm{d}u/\mathrm{d}y = 0$. The bottom wall $y = 0$ is kept no-slip: $u_\delta = 0$. At the interface $y = \delta$, both the velocity and viscous stress are continuous: $u = u_\delta$ and $\mu\ \mathrm{d}u/\mathrm{d}y = \mu_\delta\ \mathrm{d}u_\delta/\mathrm{d}y$.

The velocity profiles that satisfy the above boundary conditions are given by

$$u = -\frac{G}{2\mu}(y^2 - 2yh) + \tilde{u}, \quad u_\delta = -\frac{G}{2\mu_\delta}(y^2 - 2yh), \tag{B 1}$$

with

$$\tilde{u} = \frac{G}{2\mu}\left(1 - \frac{\mu}{\mu_\delta}\right)(\delta^2 - 2\delta h). \tag{B 2}$$

The apparent slip length λ_{app} can be found from the ratio of the 'apparent slip' velocity $u_s \equiv [u - \delta \mathrm{d}u/\mathrm{d}y]_{y=\delta}$ (extrapolated from the interface to the bottom wall) to the shear rate of the free layer $\mathrm{d}u/\mathrm{d}y|_{y=\delta}$, giving

$$\lambda_{app} = \left(\frac{u}{\mathrm{d}u/\mathrm{d}y}\right)_{y=\delta} - \delta. \tag{B 3}$$

The slip length defined by (B 3) is also similar to the effective slip length defined by Belyaev & Vinogradova (2010) for pressure-driven flow past stripes. Applying (B 1) to the above definition gives

$$\lambda_{app} = \delta\left(\frac{\mu}{\mu_\delta}\left(\frac{1 - \delta/2h}{1 - \delta/h}\right) - 1\right) \approx \delta\left(\frac{\mu}{\mu_\delta} - 1\right). \tag{B 4}$$

This leads to (4.1*a*) in agreement with that given by Vinogradova (1995). It is worth remarking that (B 4) gives a correct limit $\lambda_{app} \to 0$ as $\mu_\delta \to \mu$. De Gennes (1979) took λ_{app} to be the ratio of the interfacial velocity $u(y=\delta)$ to the wall shear rate $\mathrm{d}u/\mathrm{d}y$, and found $\lambda_{app} = (\mu/\mu_\delta)\delta$. But this only holds for $\mu/\mu_\delta \gg 1$, which of course agrees with (B 4) in that limit.

Writing the flow rate q (per unit width) across the entire film in terms of the equivalent form $q = Gh^3/3\mu_{app}$ as if the lubricating layer were absent, the apparent viscosity μ_{app} can be determined as

$$\mu_{app} = \frac{Gh^3}{3q}. \tag{B 5}$$

Integrating (B 1) from $y=0$ to $y=h$ and neglecting the terms higher than $O(\delta/h)$, q is given by

$$q \approx \frac{Gh^3}{3\mu}\left(1 + 3\left(\frac{\mu}{\mu_\delta} - 1\right)\frac{\delta}{h}\right). \tag{B 6}$$

The resulting apparent viscosity can then be found by substituting the above into (B 5):

$$\mu_{app} \approx \frac{h}{3\delta\left(\dfrac{\mu}{\mu_\delta} - 1\right) + h}\mu, \tag{B 7}$$

which leads to (4.1*b*) after replacing $\delta(\mu/\mu_\delta - 1)$ by λ_{app} using (B 4).

B.2. *Textured hydrophilic surface*

The lubricating layer here is a porous medium of permeability K_p and has the same viscosity as the bulk value μ. The flow in this layer behaves like a plug flow characterized by the Darcy law, $u_\delta = K_p G/\mu$, which has to match the velocity of the free layer at the interface $y=\delta$. The top surface $y=h$ is again stress-free: $\mathrm{d}u/\mathrm{d}y = 0$.

The resulting velocity profiles are

$$u = -\frac{G}{2\mu}(y^2 - 2yh) + \tilde{u}, \quad u_\delta = \frac{K_p}{\mu}G, \tag{B 8}$$

with

$$\tilde{u} = \frac{G}{2\mu}(\delta^2 - 2\delta h) + \frac{K_p G}{\mu}. \tag{B 9}$$

Using (B 3), the apparent slip length is found to be

$$\lambda_{app} = \frac{K_p}{h-\delta} - \delta \approx \frac{K_p}{h} - \delta, \tag{B 10}$$

which is (4.2*a*). The flow rate q based on the velocity profiles (B 8) is

$$q = \frac{G}{3\mu}(h-\delta)^3 + \frac{K_p G}{\mu}h \approx \frac{Gh^3}{3\mu}\left(1 - \frac{3\delta}{h} + \frac{3K_p}{h^2}\right). \tag{B 11}$$

The apparent viscosity can then be found using (B 5):

$$\mu_{app} \approx \frac{h\mu}{3\left(\dfrac{K_p}{h} - \delta\right) + h}. \tag{B 12}$$

This is (4.2*b*) in terms of λ_{app} using (B 10).

REFERENCES

AJDARI, A. & BOCQUET, L. 2006 Giant amplification of interfacially driven transport by hydrodynamic slip: diffusio-osmosis and beyond. *Phys. Rev. Lett.* **96**, 186102.

ALBRECHT, U., OTTO, A. & LEIDERER, P. 1992 Two-dimensional liquid polymer diffusion: experiment and simulation. *Phys. Rev. Lett.* **68**, 3192–3195.

ASMOLOV, E. S. & VINOGRADOVA, O. I. 2012 Effective slip boundary conditions for arbitrary one-dimensional surfaces. *J. Fluid Mech.* **706**, 108–117.

BEAVERS, G. S. & JOSEPH, D. D. 1967 Boundary conditions at a naturally permeable wall. *J. Fluid Mech.* **30**, 197–207.

BELYAEV, A. V. & VINOGRADOVA, O. I. 2010 Effective slip in pressure-driven flow past super-hydrophobic stripes. *J. Fluid Mech.* **652**, 489–499.

BICO, J. & QUÉRÉ, D. 2002 Self-propelling slugs. *J. Fluid Mech.* **467**, 101–127.

BOCQUET, L. & BARRAT, J. L. 2007 Flow boundary conditions from nano- to micro-scales. *Soft Matt.* **3**, 685–693.

BONACCURSO, E., BUTT, H.-J. & CRAIG, V. S. J. 2003 Surface roughness and hydrodynamic boundary slip of a Newtonian fluid in a completely wetting system. *Phys. Rev. Lett.* **90**, 144501.

BONN, D., EGGERS, J., INDEKEU, J., MEUNIER, J. & ROLLEY, E. 2009 Wetting and spreading. *Rev. Mod. Phys.* **81**, 739–805.

BRETHERTON, F. P. 1961 The motion of long bubbles in tubes. *J. Fluid Mech.* **10**, 166–188.

BROCHARD, F. & DE GENNES, P. G. 1984 Spreading laws for liquid polymer droplets: interpretation of the foot. *J. Phys. Lett.* **45**, 597–602.

BROCHARD-WYART, F., DE GENNES, P. G., HERVERT, H. & REDON, C. 1994 Wetting and slippage of polymer melts on semi-ideal surfaces. *Langmuir* **10**, 1566–1572.

BROCHARD-WYART, F., DEBRÉGEAS, G. & DE GENNES, P. G. 1996 Spreading of viscous droplets on a non viscous liquid. *Colloid Polym. Sci.* **274**, 70–72.

CASSIE, A. B. D. & BAXTER, S. 1944 Wettability of porous surfaces. *Trans. Faraday Soc.* **40**, 546–551.

COX, R. G. 1986 The dynamics of the spreading of liquids on a solid surface. Part 1. Viscous flow. *J. Fluid Mech.* **168**, 169–194.

CHEN, J.-D. 1988 Experiments on a spreading drop and its contact angle on a solid. *J. Colloid Interface Sci.* **122**, 60–72.

CHOI, C.-H. & KIM, C.-J. 2006 Large slip of aqueous liquid flow over a nanoengineered superhydrophobic surface. *Phys. Rev. Lett.* **96**, 066001.

CHOI, C.-H., ULMANELLA, U., KIM, J., HO, C.-M. & KIM, C.-J. 2006 Effective slip and friction reduction in nanograted superhydrophobic microchannels. *Phys. Fluids* **18**, 087105.

CHOI, C.-H., WESTIN, K. J. A. & BREUER, K. S. 2003 Apparent slip flows in hydrophilic and hydrophobic microchannels. *Phys. Fluids* **15**, 2897–2902.

CRAIG, V. S. J., NETO, C. & WILLIAMS, D. R. M. 2001 Shear-dependent boundary slip in an aqueous Newtonian liquid. *Phys. Rev. Lett.* **87**, 054504.

DENKOV, N. D., SUBRAMANIAN, V., GUROVICH, D. & LIPS, A. 2005 Wall slip and viscous dissipation in sheared foams: effect of surface mobility. *Colloids Surf.* A **263**, 129–145.

DEVAUCHELLE, O., JOSSERAND, C. & ZALESKI, S. 2007 Forced dewetting on porous media. *J. Fluid Mech.* **574**, 343–364.

EGGERS, J. 2004 Toward a description of contact line motion at higher capillary numbers. *Phys. Fluids* **16**, 3491–3494.

EGGERS, J. & STONE, H. A. 2004 Characteristic lengths at moving contact lines for a perfectly wetting fluid: the influence of speed on the dynamic contact angle. *J. Fluid Mech.* **505**, 309–321.

FEUILLEBOIS, F., BAZANT, M. Z. & VINOGRADOVA, O. I. 2009 Effective slip over superhydrophobic surfaces in thin channels. *Phys. Rev. Lett.* **102**, 026001.

DE GENNES, P. G. 1979 Ecoulements viscométriques de polymères enchevêtrés. *C. R. Acad. Sci. Paris* B **288**, 219–220.

DE GENNES, P. G. 1985 Wetting: statics and dynamics. *Rev. Mod. Phys.* **57**, 827–863.

DE GENNES, P. G., BROCHARD-WYART, F. & QUÉRÉ, D. 2003 *Capillarity and Wetting Phenomena: Drops, Bubbles, Pearls, Waves*. Springer.

HERVET, H. & DE GENNES, P. G. 1984 Dynamique du mouillage: films précurseurs sur solides 'sec'. *C. R. Acad. Sci. Paris* II **299**, 499–503.

HESLOT, F., CAZABAT, A. M. & LEVINSON, P. 1989 Dynamics of wetting of tiny drops: ellipsometric study of the late stages of spreading. *Phys. Rev. Lett.* **62**, 1286–1289.

HOCKING, L. M. 1976 A moving fluid interface. Part 2. The removal of the force singularity by a slip flow. *J. Fluid Mech.* **79**, 209–229.

HOFFMAN, R. L. 1975 A study of the advancing interface. Part 1. Interface shape in liquid–gas systems. *J. Colloid Interface Sci.* **50**, 228–241.

KALLIADASIS, S. & CHANG, H.-C. 1994 Apparent dynamic contact angle of an advancing gas–liquid meniscus. *Phys. Fluids* **6**, 12–23.

KALLIADASIS, S. & CHANG, H.-C. 1996 Dynamics of liquid spreading on solid surfaces. *Ind. Engng Chem. Res.* **35**, 2860–2874.

KRECHETNIKOV, R. & HOMSY, G. M. 2005 Experimental study of substrate roughness and surfactant effects on the Landau–Levich law. *Phys. Fluids* **17**, 102108.

LANDAU, L. & LEVICH, B. 1942 Dragging of a liquid by a moving plate. *Acta Physicochim. USSR* **17**, 42–54.

LAUGA, E., BRENNER, M. & STONE, H. 2007 Microfluidics: the no-slip boundary condition. In *Springer Handbook of Experimental Fluid Mechanics* pp. 1219–1240. Springer.

LAUGA, E. & STONE, H. A. 2003 Effective slip in pressure-driven Stokes flow. *J. Fluid Mech.* **489**, 55–77.

LIAO, Y.-C., LI, Y.-C. & WEI, H.-H. 2013 Drastic changes in interfacial hydrodynamics due to wall slippage: slip-intensified film thinning, drop spreading, and capillary instability. *Phys. Rev. Lett.* **111**, 136001.

LOPEZ, J., MILLER, C. A. & RUCKENSTEIN, E. 1976 Spreading kinetics of liquid drops on solids. *J. Colloid Interface Sci.* **56**, 460–468.

MATE, C. M. 2012 Anomalous diffusion kinetics of the precursor film that spreads from polymer droplets. *Langmuir* **28**, 16821–16827.

NAVIER, C. L. M. H. 1823 Mémoire sur les lois du mouvement des fluides. *Mem. Acad. Sci. Inst. Fr.* **6**, 389–440.

OSKOOEI, S. A. K. & SINTON, D. 2010 Partial wetting gas–liquid segmented flow microreactor. *Lab on a Chip* **10**, 1732–1734.

QUÉRÉ, D. 2008 Wetting and roughness. *Annu. Rev. Mater. Res.* **38**, 71–99.

RATULOWSKI, J. & CHANG, H.-C. 1989 Transport of gas bubbles in capillaries. *Phys. Fluids* A **1**, 1642–1655.

REINELT, D. A. & SAFFMAN, P. G. 1985 The penetration of a finger into a viscous fluid in a channel and tube. *SIAM J. Sci. Stat. Comput.* **6**, 542–561.

RESTAGNO, F., CRASSOUS, J., CHARLAIX, É., COTTIN-BIZONNE, C. & MONCHANIN, M. 2002 A new surface forces apparatus for nanorheology. *Rev. Sci. Instrum.* **73**, 2292–2297.

SAUGEY, A., DRENCKHAN, W. & WEAIRE, D. 2006 Wall slip of bubbles in foams. *Phys. Fluids* **18**, 053101.

SAVVA, N. & KALLIADASIS, S. 2011 Dynamics of moving contact lines: a comparison between slip and precursor film models. *Europhys. Lett.* **94**, 64004.

SBRAGAGLIA, M, BENZI, R., BIFERALE, L., SUCCI, S. & TOSCHI, F. 2006 Surface roughness–hydrophobicity coupling in microchannel and nanochannel flows. *Phys. Rev. Lett.* **97**, 204503.

SEIWERT, J., CLANET, C. & QUÉRÉ, D. 2011 Coating of a textured solid. *J. Fluid Mech.* **669**, 55–63.

SHIRTCLIFFE, N. J., MCHALE, G., ATHERTON, S. & NEWTON, M. I. 2010 An introduction to superhydrophobicity. *Adv. Colloid Interface Sci.* **161**, 124–138.

SONG, H., TICE, J. D. & ISMAGILOV, R. F. 2003 A microfluidic system for controlling reaction networks in time. *Angew. Chem. Intl Ed. Engl.* **42**, 768–772.

STONE, H. A. 2010 Interfaces: in fluid mechanics and across disciplines. *J. Fluid Mech.* **645**, 1–25.

TANNER, L. H. 1979 The spreading of silicone oil drops on horizontal surfaces. *J. Phys.* D **12**, 1473–1484.

TELETZKE, G. F., DAVIS, H. D. & SCRIVEN, L. E. 1988 Wetting hydrodynamics. *Rev. Phys. Appl. (Paris)* **23**, 989–1007.

TRETHEWAY, D. C. & MEINHART, C. D. 2002 Apparent fluid slip at hydrophobic microchannel walls. *Phys. Fluids* **14**, L9–L12.

TSAI, P., PETERS, A. M., PIRAT, C., WESSLING, M., LAMMERTINK, R. G. H. & LOSHE, D. 2009 Quantifying effective slip length over micropatterned hydrophobic surfaces. *Phys. Fluids* **21**, 112002.

TYRRELL, J. W. G. & ATTARD, P. 2001 Images of nanobubbles on hydrophobic surfaces and their interactions. *Phys. Rev. Lett.* **87**, 176104.

VINOGRADOVA, O. I. 1995 Drainage of a thin liquid film confined between hydrophobic surfaces. *Langmuir* **11**, 2213–2220.

WENZEL, R. N. 1936 Resistance of solid surfaces to wetting by water. *Ind. Engng Chem.* **28**, 988–994.

XU, H., SHIRVANYANTS, D., BEERS, K., MATYJASZEWSKI, K., RUBINSTEIN, M. & SHEIKO, S. S. 2004 Molecular motion in a spreading precursor film. *Phys. Rev. Lett.* **93**, 206103.

YBERT, C., BARENTIN, C., COTTIN-BIZONNE, C., JOSEPH, P. & BOCQUET, L. 2007 Achieving large slip with superhydrophobic surfaces: scaling laws for generic geometries. *Phys. Fluids* **19**, 123601.

YEO, L. Y. & CHANG, H.-C. 2006 Electrowetting films on parallel line electrodes. *Phys. Rev. E* E **73**, 011605.

ZHU, Y. & GRANICK, S. 2001 Rate-dependent slip of Newtonian liquid at smooth surfaces. *Phys. Rev. Lett.* **87**, 096105.